*energies*

MDPI

*Article*

# Synthesis and Electrochemical Properties of the $Li_3PO_4$-Coated $LiNi_{0.5}Mn_{1.5}O_4$ Cathode Materials for High-Voltage Lithium-Ion Batteries

**So Young Choi, Jong Hun Sung, Fuead Hasan, Sangram Keshari Mohanty, Madhusudana Koratikere Srinivasa and Hyun Deog Yoo ***

Department of Chemistry and Chemical Institute for Functional Materials, Pusan National University, Busan 46241, Republic of Korea; chlthdud99@gmail.com (S.Y.C.); jonghun.sung@dgist.ac.kr (J.H.S.); fhasan1@charlotte.edu (F.H.); mohantysangram656@gmail.com (S.K.M.); ksmchem28@pusan.ac.kr (M.K.S.)
* Correspondence: hyundeog.yoo@pusan.ac.kr

**Abstract**

High-voltage spinel ($LiNi_{0.5}Mn_{1.5}O_4$; LNMO) has been a prospective cathode material that may exploit the maximal voltage of 5 V for lithium-ion batteries. However, the practical application has been hindered by the severe electrochemical instability of the $Ni^{2+}/Ni^{4+}$ redox couple at such a high voltage. Herein, we coated lithium phosphate ($Li_3PO_4$) on the surface of the LNMO by a wet-coating method to improve the electrochemical stability. The coating layer provided an effective cathode–electrolyte interphase, which prevented the excessive decomposition of the electrolyte on the surface of LNMO cathode. The $Li_3PO_4$-coated LNMO exhibited enhanced rate capability in accordance with the lowered solid-electrolyte interphase (SEI) and charge-transfer resistance values from electrochemical impedance spectroscopy.

**Keywords:** high-voltage spinel cathode; Li-ion battery; lithium phosphate coating

check for updates

Academic Editors: Zbigniew Łodziana and Bahareh Khezri

Received: 31 March 2025
Revised: 11 June 2025
Accepted: 24 June 2025
Published: 27 June 2025

**Citation:** Choi, S.Y.; Sung, J.H.; Hasan, F.; Mohanty, S.K.; Srinivasa, M.K.; Yoo, H.D. Synthesis and Electrochemical Properties of the $Li_3PO_4$-Coated $LiNi_{0.5}Mn_{1.5}O_4$ Cathode Materials for High-Voltage Lithium-Ion Batteries. *Energies* **2025**, *18*, 3387. https://doi.org/10.3390/en18133387

**Copyright:** © 2025 by the authors. Licensee MDPI, Basel, Switzerland. This article is an open access article distributed under the terms and conditions of the Creative Commons Attribution (CC BY) license (https://creativecommons.org/licenses/by/4.0/).

## 1. Introduction

With recent advances in electric vehicles (EVs), hybrid electric vehicles (HEVs), and large-scale energy storage systems (ESSs), lithium-ion batteries (LIBs) have been considered as one of the most promising candidates for energy storage [1–3]. Enhancing LIBs' energy density is highly desirable to meet a wide range of needs, from longer usage of portable electronics to practical electromobility [4–6]. The energy and power densities of LIBs are mainly determined by the voltage and capacity of the cathode materials [7,8]. While Ni-rich cathodes such as $LiNi_{1-x-y}Co_xMn_yO_2$ (NCM) and $LiNi_{1-x-y}Co_xAl_yO_2$ (NCA) offer relatively higher energy density, lithium iron phosphate ($LiFePO_4$; LFP) cathodes are becoming more important due to better safety despite the lower energy density. For futuristic cathode materials, it is highly preferrable to have higher operational potential without using expensive and toxic elements such as cobalt. In this regard, high-voltage spinel $LiNi_{0.5}Mn_{1.5}O_4$ (LNMO) has drawn much attention due to the high operational voltage of ca. 4.7 V vs. $Li/Li^+$, low cost, and manganese's environmentally friendly properties [2,9,10]. The high operational voltage is due to the active redox couples of $Mn^{3+}/Mn^{4+}$ and $Ni^{2+}/Ni^{4+}$ at ca. 4.0 and 4.7 V vs. $Li/Li^+$, respectively [11]. With the specific capacity of more than 140 mAh $g^{-1}$, the maximum energy density reaches 650 Wh $kg^{-1}$, which exceeds that of $LiCoO_2$, $LiMn_2O_4$, and $LiFePO_4$ materials [12,13]. In addition, the three-dimensional crystal structure offers a high rate capability [3,14].

However, the high-voltage spinel cathode suffers from electrochemical instability at such high operational voltage, which often leads to the formation of impurity rock salt ($Li_yNi_{1-y}O$) phases. At the same time, hydrofluoric acid (HF) from the electrolyte decomposition elutes the transition metals from the cathode material as follows [15]:

$$LiPF_6 \rightleftarrows LiF + PF_5 \quad (1)$$

$$PF_5 + H_2O \rightarrow 2HF + POF_3 \quad (2)$$

$$2LiNi_{0.5}Mn_{1.5}O_4 + 4HF \rightarrow 3Ni_{0.25}Mn_{0.75}O_2 + 0.25NiF_2 + 0.75MnF_2 + 2LiF + 2H_2O \quad (3)$$

To mitigate the side reactions, many researchers have coated the high-voltage spinel with various metal oxides [15–25]; also, doping multivalent ions has been effective to improve the structural stability [10,23,26–30]. Lithium phosphate ($Li_3PO_4$) can suppress side reactions between the cathode material and the electrolyte by scavenging hydrofluoric acid (HF), while the relatively high $Li^+$ conductivity ($1.7 \times 10^{-9}$ S $cm^{-1}$) can mitigate the adverse impact on $Li^+$ transport kinetics. As a result, $Li_3PO_4$ has been utilized as an effective coating agent for stable interphase in Li-ion batteries [31–54]; however, investigations are ongoing to reveal exact roles, efficient methods, and the optimal level of $Li_3PO_4$ coating for stabilizing the high-voltage spinel LNMO cathodes [55–60].

In this work, the $Li_3PO_4$ coating was realized via a straightforward wet-coating method in contrast to conventional techniques such as atomic layer deposition (ALD) [58,61], physical vapor deposition (PVD) [62], pulsed laser deposition (PLD) [63,64], or solid-state reactions, which typically require expensive equipment and sophisticated processes. The proposed method is cost-effective, scalable, and flexible in terms of equipment and precursor selection, making it highly suitable for industrial implementation. The optimal level of coating was found to be 1 wt% $Li_3PO_4$ to ensure effective surface protection while minimizing the film and charge transfer resistance. The $Li_3PO_4$-coated high-voltage spinel cathode exhibited a less-severe formation of cathode–electrolyte interphase (CEI), resulting in higher thermo-electrochemical stability and enhanced rate capability due to the smaller charge transfer resistance. This approach not only improves electrochemical performance under ambient conditions but also significantly enhances cycling stability and capacity retention at an elevated temperature of 60 °C. This is, to the best of our knowledge, the first direct demonstration that $Li_3PO_4$ coating can positively contribute to the high-temperature stability of LNMO for the practical application.

## 2. Methods and Materials

### *2.1. The Synthesis of $LiNi_{0.5}Mn_{1.5}O_4$ Cathode Materials*

The $LiNi_{0.5}Mn_{1.5}O_4$ (LNMO) powders of 5 g were synthesized by a sol–gel method. A solution of citric acid (CA; DAE JUNG, Busan, Republic of Korea, 99.5%) and ethylene glycol (EG; DAE JUNG, 99.5%) in a molar ratio of 1:4 was stirred on a hot plate at 80 °C for 30 min. The stoichiometric amount of $Li(CH_3COO)_2{\cdot}2H_2O$ (DAE JUNG, 99.0%), $Mn(CH_3COO)_2 \cdot 4H_2O$ (DAE JUNG, 98.0%), and $Ni(CH_3COO)_2 \cdot 4H_2O$ (JUNSEI, Tokyo, Japan, 97.0%) were dissolved in deionized water. The metal salts' solution was slowly dropped to CA+EG solution for homogeneous reaction in a molar ratio of 1:1. Here, homogeneous reaction refers to the uniform mixing and complexation of metal salts with citric acid and ethylene glycol, ensuring even distribution of metal ions before esterification. It was then transferred into a pre-heated (380 °C) stainless beaker for further esterification, which resulted in a viscous sol. The homogenized precursor was grounded and placed in an alumina tray for calcination at 300 °C for 1 h before final sintering at 900 °C for 10 h

in a muffle furnace (FHX-05; DAIHAN Scientific, Inc., Wonju, Republic of Korea). All the calcination and sintering were carried out in an air atmosphere.

### 2.2. The Synthesis of $Li_3PO_4$-Coated $LiNi_{0.5}Mn_{1.5}O_4$ Cathode Materials

Figure 1 illustrates the process of coating Li3PO4 on LNMO particles. The coating solution was prepared by dissolving stoichiometric amount of $NH_4H_2PO_4$ (DAEJUNG Co., 98.0%) and $LiNO_3$ (DAEJUNG Co., 98.0%) in isopropyl alcohol (DAEJUNG Co., 99.7%) under sonication for 4 h and subsequent stirring at 900 rpm for 12 h. The LNMO powder was mixed with the solution under stirring for 12 h. The coated particles were filtered, washed, and dried at 100 °C under vacuum for 12 h. The coated powder was placed in an alumina tray and calcined at 300 °C for 5 h in a muffle furnace. The resultant materials were labeled as bare-LNMO, LP1-LNMO, and LP2-LNMO for 0 wt%, 1 wt%, and 2 wt% coating of lithium phosphate (LP), respectively. To achieve the targeted mass loading of $Li_3PO_4$ on LNMO particles, 0.091 g of $LiNO_3$ and 0.057 g of $NH_4H_2PO_4$ were added to the coating solution per 5.00 g of LNMO for the LP1-LNMO sample. These quantities were adjusted proportionally for LP2-LNMO, which contains a two times higher mass loading of $Li_3PO_4$ compared to LP1-LNMO.

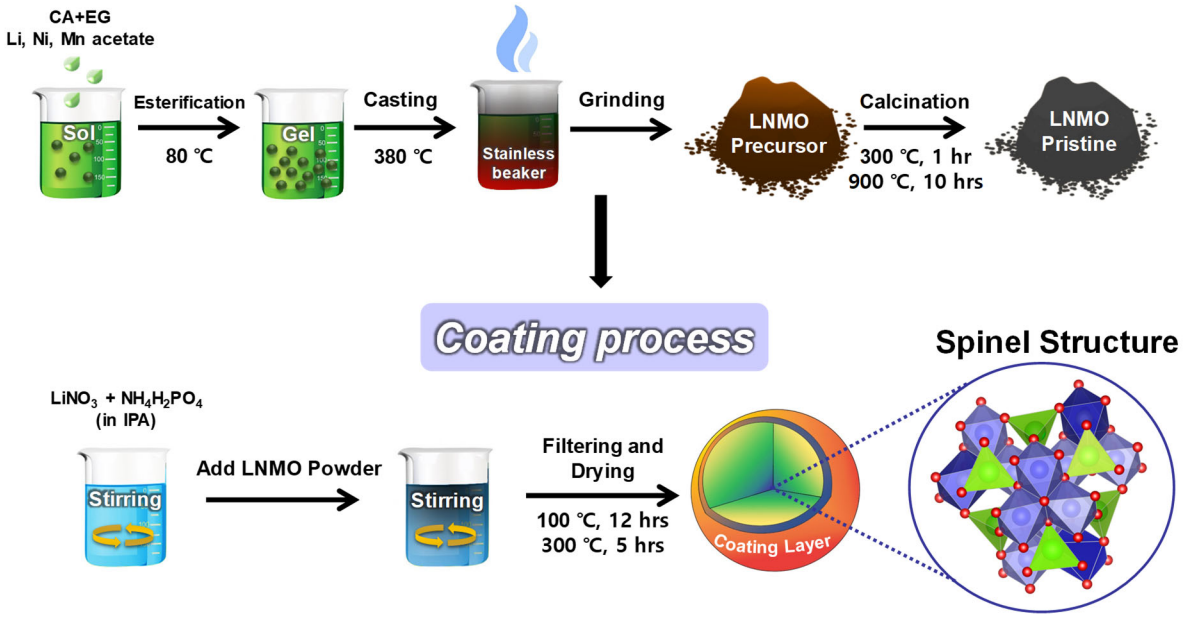



**Figure 1.** Schematic of the preparation process of bare LNMO and $Li_3PO_4$-coated LNMO.

### 2.3. Material Characterization

The crystal structure of the material was characterized by X-ray diffraction (XRD; Miniflex-600; Rigaku Co., Tokyo, Japan) using monochromatic Cu $K\alpha$ radiation in the range of 10° to 80° (2θ) with a step width of 0.02° and scanning speed of 10° $min^{-1}$. Rietveld analysis of the diffraction data of the samples was performed using PDXL2 software (version 2.8.4.0, Rigaku Co.). The morphology of the samples was imaged using a scanning electron microscope (SEM; VEGA 3; TESCAN Co., Brno, Czech Republic). Transmission electron microscopy (TEM; TALOS F200X; Thermo Fisher Scientific Inc., Walham, MA, USA) was used to identify the coating layer; and the elemental information was also obtained by energy dispersive spectroscopy (EDS) that were attached to the TEM instrument. The strong adhesion and retention of the $Li_3PO_4$ coating on LNMO particles are attributed to both its low solubility ($K_{sp} = 2.0 \times 10^{-9}$), which prevents removal during washing, and thermal treatment at 300 °C, which promotes densification and stability of the coating. During synthesis, precursor ions adsorb onto the LNMO surface, and calcination converts

them into a uniform phosphate layer. After washing and drying, post-treatment HR-TEM, SEM, and EDS analyses confirm that the coating remains intact, completely covering the LNMO surface.

### 2.4. Electrochemical Performance

For fabrication of electrodes, slurry was prepared by mixing the cathode active material (80 wt%), super-P (10 wt%, as a conductive agent), and a dispersion of polyvinylidene fluoride (10 wt%, as a binder) in N-methyl-2-pyrrolidone (Sigma Aldrich Co., St. Louis, MO, USA, 99.5%). The slurry was casted on aluminum foil using a doctor blade (Hohsen Co., Tokyo, Japan) and dried in a vacuum oven at 80 °C for 2 h, followed by punching out to form a cathode with a diameter of 11 mm. The coated film represents an interconnected network of active materials, binder, and conductive agent of uniform thickness (Figure S1). Then, 2032-type coin cells (Hohsen Co.) were assembled in the Ar-filled glove box using the cathode and a lithium foil anode that sandwiched a separator film (Separator-2400; Celgard Co., Charlotte, NC, USA) soaked with the electrolyte of 1 M $LiPF_6$ in EC:EMC (3:7 *w*/*w*; PanaXetec Co., Busan, Republic of Korea). The electrode loading of the cathodes was approximately 3 mg/cm$^2$. The galvanostatic charge and discharge characteristics of the cell were tested using a battery tester (WBCS3000L32; WonATech Co., Seoul, Republic of Korea) at a voltage range of 3.5–4.9 V at different C-rates based on the theoretical capacity of 146.7 mAh/g. Electrochemical impedance spectroscopy (EIS) measurement was performed with root mean square (rms) amplitudes of 5 mV and in the frequency range from 1 MHz to 10 mHz; and the results were fitted with an equivalent circuit using ZView software (version 3.2c, Scribner Co., Southern Pines, NC, USA).

## 3. Results and Discussion

$LiNi_{0.5}Mn_{1.5}O_4$ (LNMO) were synthesized by the sol–gel method [8,65,66]. In the sol-gel process, citric acid is used as a chelating agent that binds the metal cations for the uniform distribution in the gel precursor [67]. During the heat treatment, the chelating agent can reduce the particle size for improved electrochemical performance by shortening the diffusion path of $Li^+$ ion [68].

Figure 2 shows the X-ray diffraction (XRD) characterization of the synthesized materials. Figure 2a represents the Rietveld analysis of bare-LNMO, which exhibited a cubic spinel structure with a space group of *Fd*3*m* (Table 1) [8,69,70]. The electron conductivity of *P*4$_3$32(ordered) spinel is $10^{-7}$ S/cm, while the *Fd*3*m*(disordered) spinel is $10^{-4}$ S/cm, which leads to better rate capability [66]. Because of the disordered feature of Ni and Mn, additional electron hopping pathways may occur in contrast with *P*4$_3$32 phase [11]. Figure 2b shows the XRD patterns of all the samples, indicating the successful synthesis of LNMO cathode with sufficient crystallinity. The small peaks appearing at (440) and (400) indicate the presence of secondary phases such as $LiNi_{1-x}O$ because a small portion of oxygen is lost when LNMO is calcinated above 650 °C [20,26]. The XRD patterns of bare- and $Li_3PO_4$-coated LNMO were largely equivalent, and a peak indicating $Li_3PO_4$ was not observed due to the amorphous characteristics [71,72]. The LNMO particles exhibit well-developed polyhedral crystals less than 10 μm in size (Figure 3a) in line with the highly crystalline XRD patterns; the polyhedral morphology improves the electrochemical performance of LNMO by shortening the diffusion path of $Li^+$ ion [15]. While the overall morphology of LP1-LNMO was similar to bare-LNMO, the surface of LP1-LNMO was covered with fine particles of several nanometers in size (Figure 3b). The micro-sized (~5 μm) $LiNi_{0.5}Mn_{1.5}O_4$ particles used in this study offer advantages in tap density and reduced side reactions, making them suitable for applications prioritizing volumetric energy density and long-term stability [73–77]. In the case of LNMO-LP1, a significant amount

of phosphorus was detected on the particle surface, supporting the successful coating of $Li_3PO_4$ (Figure S2).

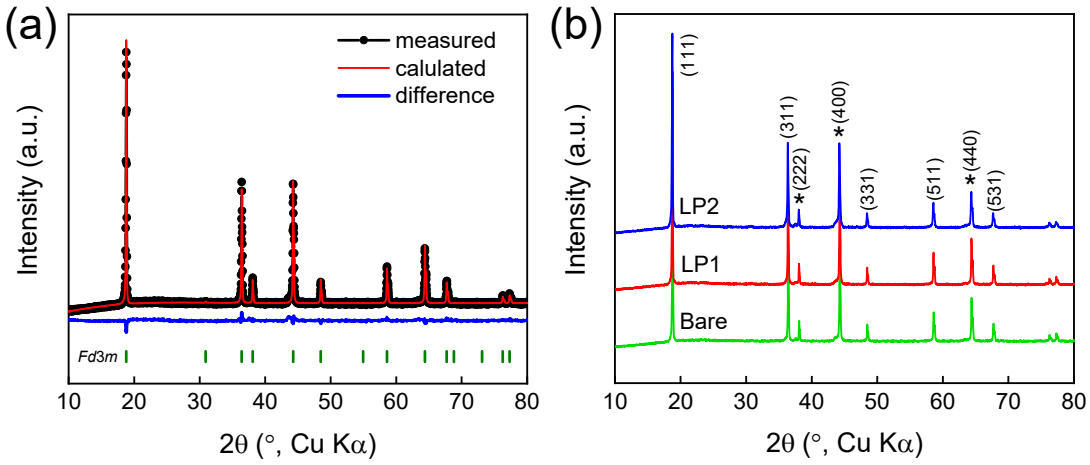



**Figure 2.** (**a**) Rietveld refinement results of bare-LNMO and (**b**) XRD patterns of bare- and $Li_3PO_4$-coated LNMO; here, asterisk (*) denotes $LiNi_{1-x}O$ phase.

**Table 1.** The Rietveld refinement results of bare- and $Li_3PO_4$-coated LNMO.

| Sample | *a* (Å) | *b* (Å) | *c* (Å) | *S* | $R_{wp}$ (%) |
|---|---|---|---|---|---|
| bare-LNMO | 8.1834 | 8.1834 | 8.1834 | 1.2978 | 3.99 |
| LP1-LNMO | 8.1813 | 8.1813 | 8.1813 | 1.2950 | 3.98 |
| LP2-LNMO | 8.1803 | 8.1803 | 8.1803 | 1.1701 | 3.66 |

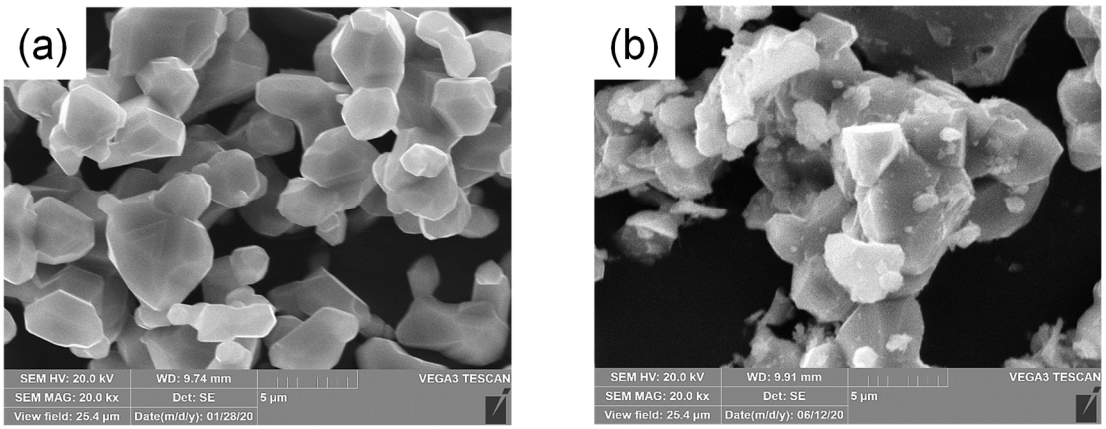



**Figure 3.** SEM images of (**a**) bare-LNMO and (**b**) LP1-LNMO.

Figure 4 shows TEM images to further identify the $Li_3PO_4$ layer coated on the surface of the LNMO particles. Figure 4a,b show the coating layers on the surfaces of LP1-LNMO and LP2-LNMO, respectively [21,24]. The thickness of the coating layers were 14 nm and 40 nm for LP1-LNMO and LP2-LNMO, respectively, indicating that thicker $Li_3PO_4$ layer was formed on the surface as the amount of coating agent increased. EDS elemental mapping confirms the presence of phosphorus and transition metals over the particles, indicating that $Li_3PO_4$ coating covers the LNMO surface completely (Figure 4c–e). The successful incorporation of the $Li_3PO_4$ layer on LNMO particles was confirmed by EDS analysis, which revealed the presence of phosphorus exclusively in the coated sample (Figures S2 and S3). Quantitative EDS analysis revealed a phosphorus-to-nickel atomic

ratio of 2.4 at% that corresponds to approximately 0.76 wt% $Li_3PO_4$ per formula unit of LNMO, which is close to the targeted value of 1 wt%.

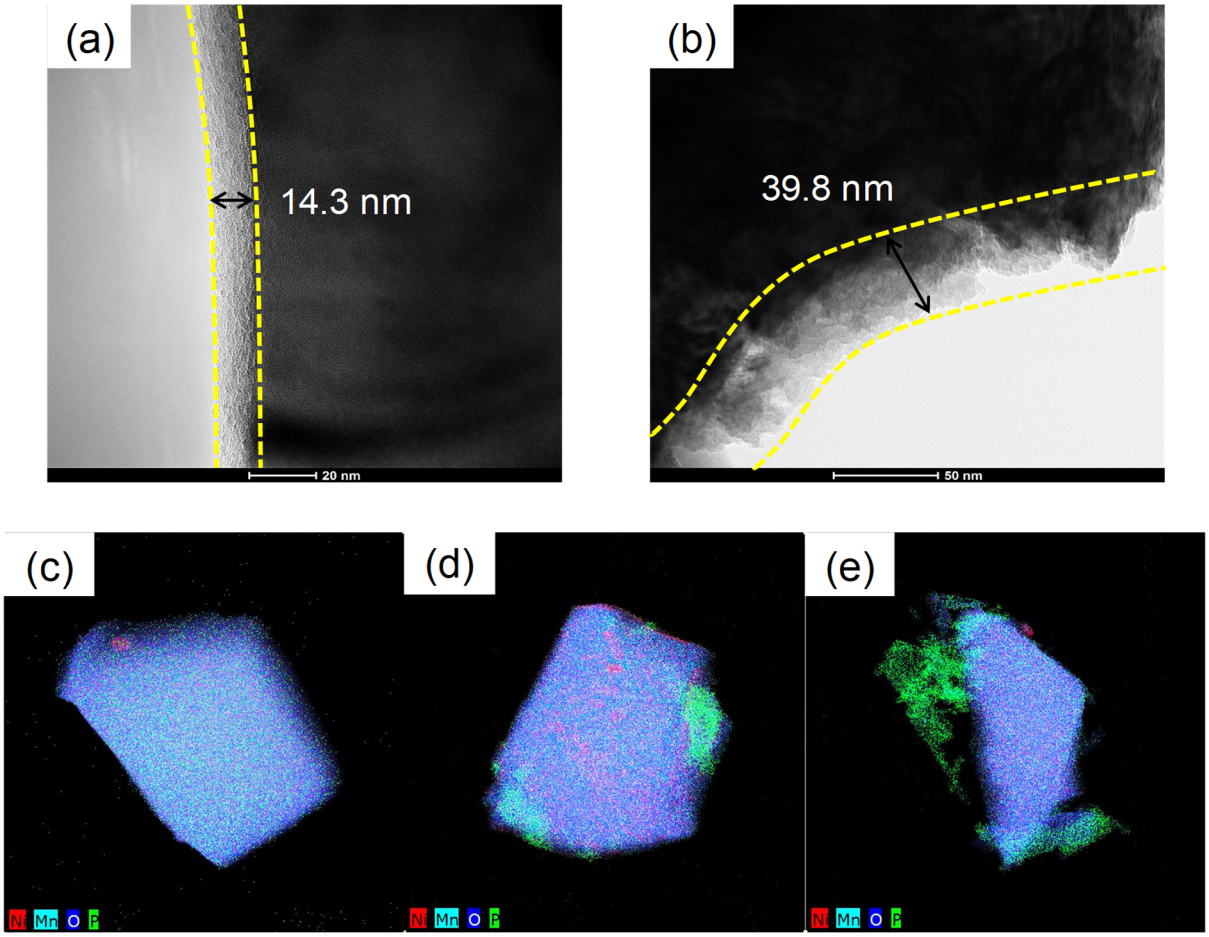



**Figure 4.** HR-TEM images of (**a**) LP1-LNMO and (**b**) LP2-LNMO. Elemental maps of (**c**) bare-LNMO, (**d**) LP1-LNMO, and (**e**) LP2-LNMO.

Figure 5a,b represent the voltage profiles of the LNMO samples at 25 °C and 60 °C, respectively. The plateau at 4.0 V is due to the redox reaction of $Mn^{3+}/Mn^{4+}$, and the plateau at 4.7 V is due to the redox reaction of $Ni^{2+}/Ni^{3+}/Ni^{4+}$, in accordance with previously reported LNMO cathodes with *Fd*3*m* spinel structure [7,18]. The cathode capacity decreases with increasing $Li_3PO_4$ thickness as $Li_3PO_4$ constitutes additional mass that does not participate in the intercalation reaction. Despite this aspect, the coated electrodes demonstrate improved rate capability and thermal stability, suggesting potential for further optimization. Bare-LNMO and $Li_3PO_4$-coated LNMO exhibit similar plateaus, implying that $Li_3PO_4$ does not participate in the electrochemical reaction during the electrochemical cycling. Previous studies have shown that phosphorus incorporation into the bulk lattice modifies the voltage profile due to structural changes [78]. In this study, the voltage profiles of bare-LNMO, LP1-LNMO, and LP2-LNMO remain nearly identical, indicating that $Li_3PO_4$ resides on the surface rather than being doped into the bulk. This confirms that the coating does not participate directly in the redox process. Instead, the $Li_3PO_4$ layer acts as a passivation layer, enhancing thermo-electrochemical stability while preserving the rate capability due to its moderate $Li^+$ ionic conductivity ($1.7 \times 10^{-9}$ S $cm^{-1}$). At 25 °C, bare-LNMO, LP1-LNMO, and LP2-LNMO exhibit discharge capacities of 124.5, 121.3, and 111.7 mAh/g, respectively. On the other hand, the discharge capacities at 60 °C are 110.2, 143.1, and 109.2 mAh/g, respectively. This observation evidences that the discharge capacity of the

cathode materials significantly decreases as the loading amount of coating agent increases over 1 wt%. Such thicker coating layer may act like an insulating shell that hinders the ionic transport [15]. Figure 5c,d show cycle performances of the samples at 25 °C and 60 °C, respectively; at 25 °C, all the samples exhibit fairly stable cycling performances (Figure 5c). However, at the elevated temperature of 60 °C, bare-LNMO experiences severe capacity fading (Figure 5d), due to the accelerated dissolution of transition metals and electrolyte decomposition, resulting in severer HF attack. On the other hand, $Li_3PO_4$-coated LNMO samples exhibit more stable cycle performance at 60 °C, supporting that $Li_3PO_4$ coating layer provided a protecting layer on the surface of LNMO particles, preventing the structural collapse and the electrolyte decomposition during the high-voltage operation [72]. Figure 5e,f represent the voltage hysteresis profiles of the LNMO samples at 25 °C and 60 °C, respectively. Bare-LNMO samples exhibit significantly reduced capacity at 60 °C, especially for $Mn^{3+}/Mn^{4+}$ redox couple. This observation provides a strong evidence of the manganese dissolution during the electrochemical cycling at the elevated temperature of 60 °C [4,79].

All samples maintained reasonable coulombic efficiency (CE) at room temperature (~97% at 0.05C and ~99% at 1C), but the effects of the coating became more pronounced at the elevated temperature of 60 °C (Table S1). The bare sample exhibited a sharp drop in CE to 59.2%, indicating significant parasitic reactions. In contrast, the 1 wt% and 2 wt%-coated samples maintained higher CE values of 76.5% and 72.8%, respectively, confirming that the $Li_3PO_4$ coating effectively suppresses side reactions at elevated temperatures. These results demonstrate that $Li_3PO_4$ coatings enhance coulombic efficiency, particularly under thermally and kinetically challenging conditions.

Differential capacity ($dQ/dV$) plots visualize the redox reactions of $Mn^{3+}/Mn^{4+}$ (4.0 V vs. $Li/Li^+$) and $Ni^{2+}/Ni^{3+}/Ni^{4+}$ (4.7 V vs. $Li/Li^+$) during the phase changes of the LNMO cathodes upon repeated cycling at 25 °C and 60 °C (Figure 6). The $dQ/dV$ plots of $Li_3PO_4$-coated LNMO samples exhibit larger overpotential compared to bare LNMO, especially upon lithiation (discharging process); among the $Li_3PO_4$-coated LP1- and LP2-LNMO samples, LP2-LNMO with the larger amount of $Li_3PO_4$ coating brings about larger overpotential compared with LP1-LNMO. These observations imply that the coating layer effectively protects the active materials, accompanying with the hindered ionic transport especially during the lithiation of active materials. Although there were no significant differences in the electrochemical characteristics during the initial cycles at 25 °C and 60 °C, bare LNMO suffered from noticeable degradation after 30 cycles at 60 °C. These observations evidence the effectiveness of the $Li_3PO_4$ coating to mitigate the side reactions on the electrode surface during the operation of LNMO cells at higher temperature.

Figure 7 shows the rate capability of all LNMO samples at various C-rates from 0.05C to 5C at 25 °C. As shown in Figure 7a,b, LP1-LNMO sample exhibited the best capacity retention up to the 5C rate, suggesting that the $Li_3PO_4$ coating of moderate thickness enhances the rate performance of LNMO cathodes. The capacity values of bare LNMO were 129.2 and 4.6 mAh $g^{-1}$ at 0.05C and 5C, respectively; on the other hand, the capacity values of LP1-LNMO were 123.8 and 43.7 mAh $g^{-1}$ at 0.05C and 5C rate, respectively. This improved rate capability can be due to the enhanced ionic transport by coating Li-ion conducting $Li_3PO_4$, which provides stable CEI by protecting the electrode surface from the side reactions at higher electrode potential. However, LP2-LNMO with an excessive coating layer exhibited the worst rate capability probably due to the blockage of the path for charge transfer reaction as the electron tunneling becomes exponentially challenging as the thickness of insulating layer increases [15]. As a result, the highest rate capability was achieved for LP1-LNMO with a moderate thickness of $Li_3PO_4$ coating, emphasizing the importance of the optimal thickness of the coating layer for higher rate capability.

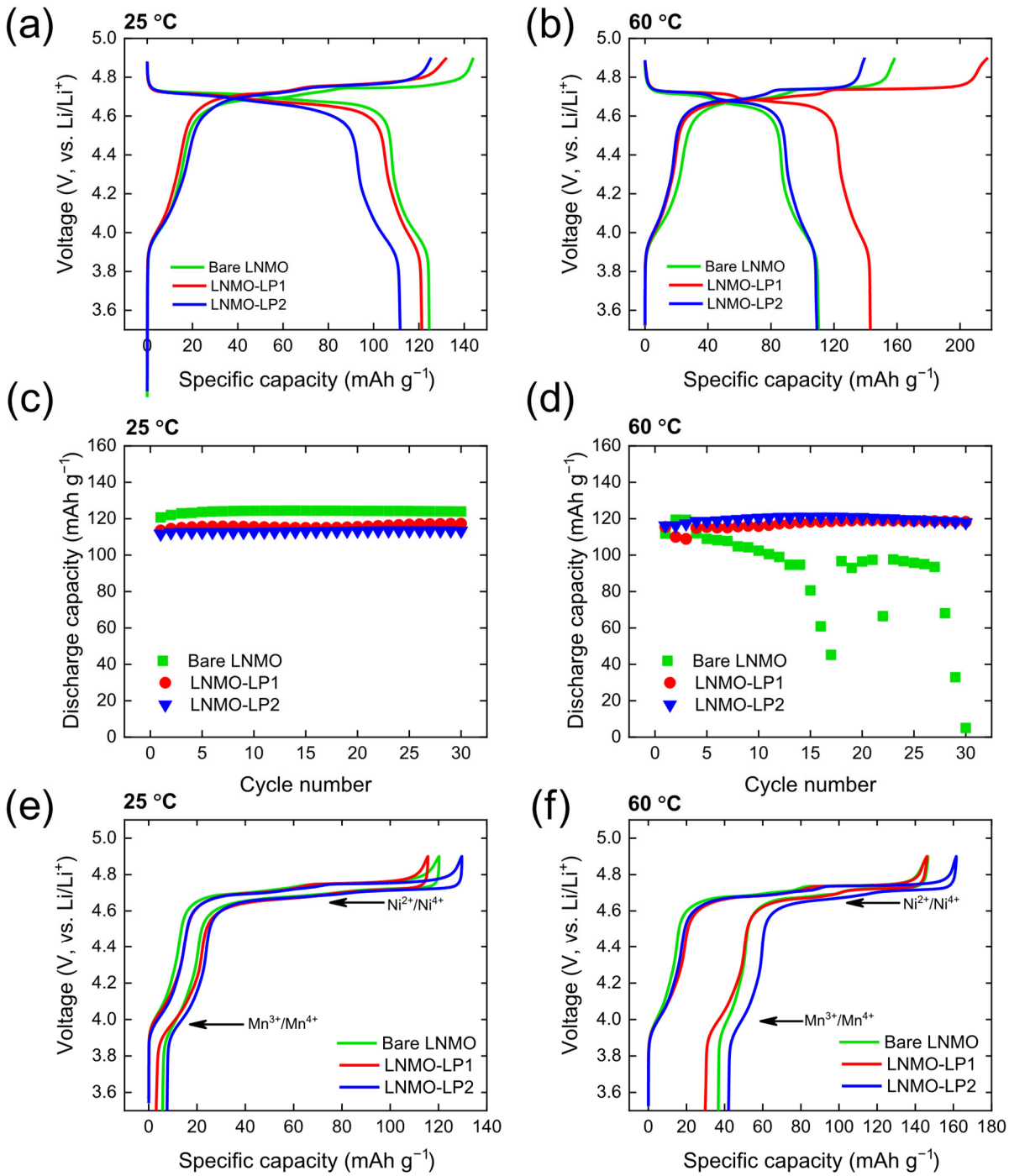



**Figure 5.** The charge–discharge curves at (**a**) 25 °C and (**b**) 60 °C. Cycling performance at 0.05C at (**c**) 25 °C and (**d**) 60 °C. Hysteresis plots LNMO electrodes at (**e**) 25 °C and (**f**) 60 °C.

To investigate the detailed effect of $Li_3PO_4$ coating on LNMO, electrochemical impedance spectroscopy (EIS) analysis was conducted before and after 30 cycles at 25 °C and 60 °C (Figure 8). The lithium-ion diffusion coefficients of LNMO cathodes were evaluated using EIS data (Table S2), revealing an order-of-magnitude lower $Li^+$ diffusivity for LP-coated LNMO. This is consistent with literature reports indicating that surface-passivating coatings, while enhancing interfacial stability, often introduce additional interfacial resistance and hinder lithium transport kinetics. The EIS data was fitted by the equivalent circuit of Figure 8d, and the temperature-specific resistance values obtained by fitting are given in Tables 2 and 3. The equivalent circuit comprises the electrolyte solution resistance ($R_{sol}$),

SEI film resistance ($R_{film}$), the charge transfer resistance ($R_{ct}$), and the Warburg impedance, which is related with the solid-state $Li^+$ ion diffusion [14,21]. Before cycling, there was no clear tendency in the size of semi-circle resistance that includes $R_{film}$ and $R_{ct}$; in fact, LP1-LNMO exhibited the largest resistance among them. However, the repeated cycling of bare LNMO cells resulted in substantially increased $R_{film}$ and $R_{ct}$ values, which were 1~2 orders of magnitude larger than $Li_3PO_4$-coated LNMO cells, both at 25 °C and 60 °C. At 25 °C, $R_{film}$ and $R_{ct}$ of LP1-LNMO after 30 cycles were 11.8 Ω and 8.5 Ω, respectively, which were significantly lower than 90 Ω and 390 Ω for bare LNMO. Cycling at 60 °C aggravated bare LNMO severely, resulting in even larger $R_{film}$ and $R_{ct}$ values of 2232 Ω and 12,000 Ω, which were substantially larger than 13 Ω and 2890 Ω for LP1-LNMO in the equivalent condition. These observations suggest that 1 wt% of $Li_3PO_4$ coating effectively suppressed the formation of excessive SEI film, ensuring more stable interphase during the repeated cycling, especially at the elevated temperature of 60 °C.

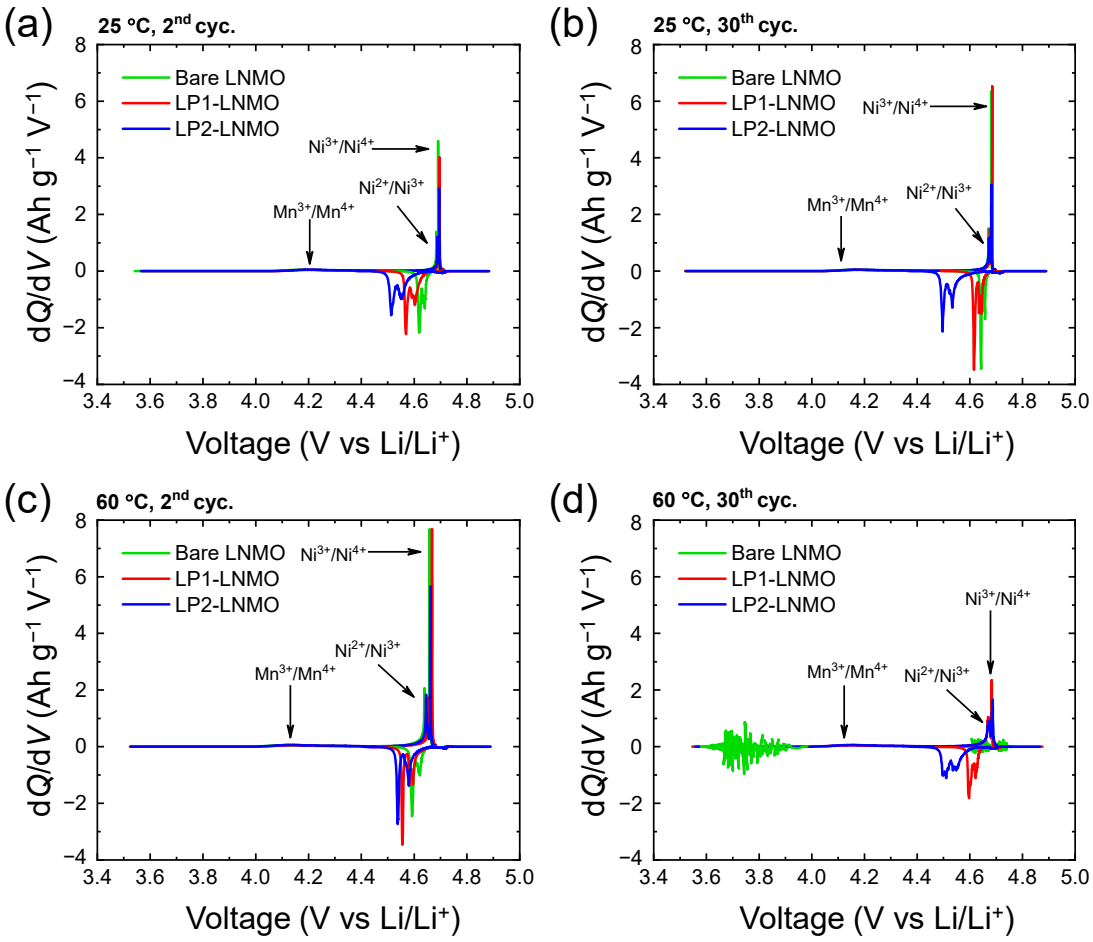



**Figure 6.** d$Q$/d$V$ plots of bare and LP-coated LNMO cells: after cycling at 25 °C for (**a**) 2 and (**b**) 30 cycles and after cycling at 60 °C for (**c**) 2 and (**d**) 30 cycles.

**Table 2.** Fitted parameters of EIS data after 30 cycles at 25 °C.

| | $R_{sol}$ (Ω) | $R_{film}$ (Ω) | $R_{ct}$ (Ω) |
|---|---|---|---|
| Bare LNMO | 2.41 ± 0.06 | 90 ± 1 | 390 ± 30 |
| LP1-LNMO | 2.50 | 11.8 ± 0.6 | 8.5 ± 0.6 |
| LP2-LNMO | 1.90 ± 0.05 | 67 ± 6 | 18 ± 6 |

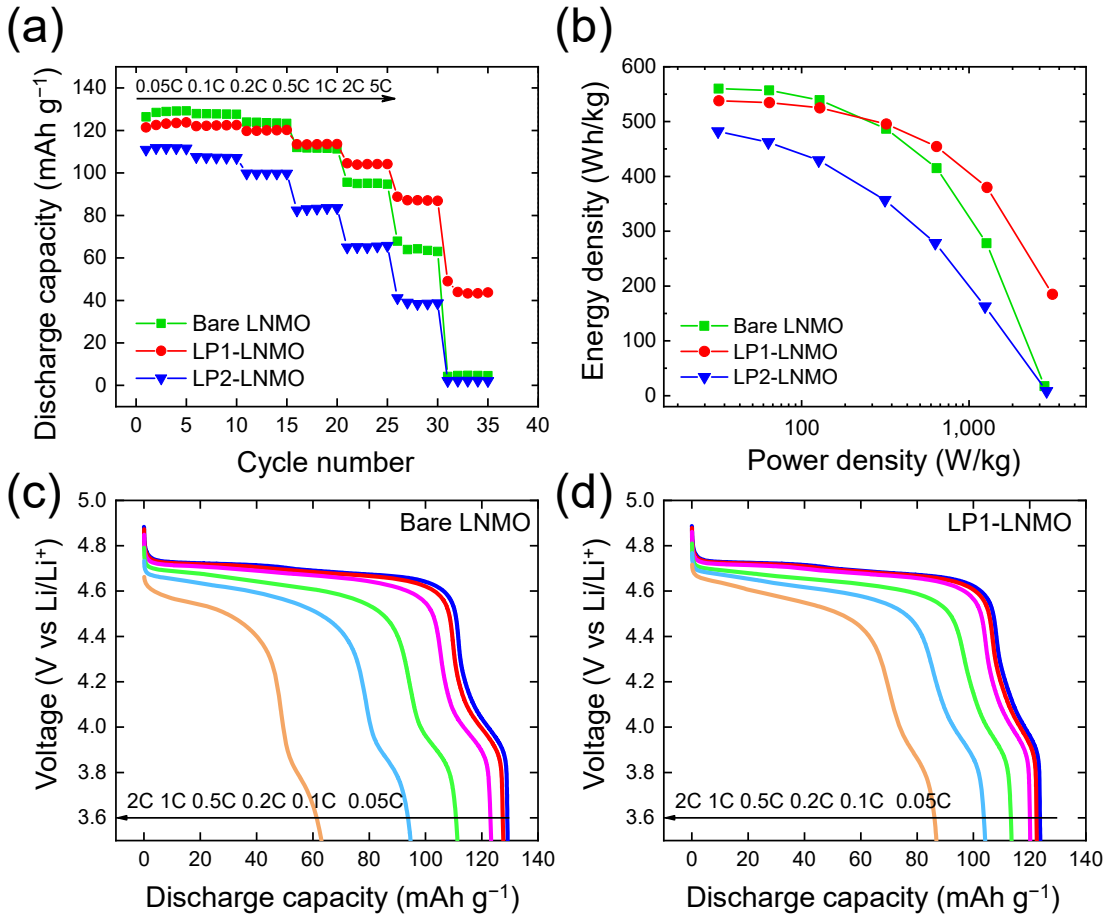



**Figure 7.** Rate capability of LNMO electrodes with different level of $Li_3PO_4$ coating: (**a**) discharge capacity and (**b**) the relative capacity retention at varied C-rates at 25 °C. Discharge curves at different C-rates for (**c**) bare-LNMO and (**d**) LP1-LNMO.

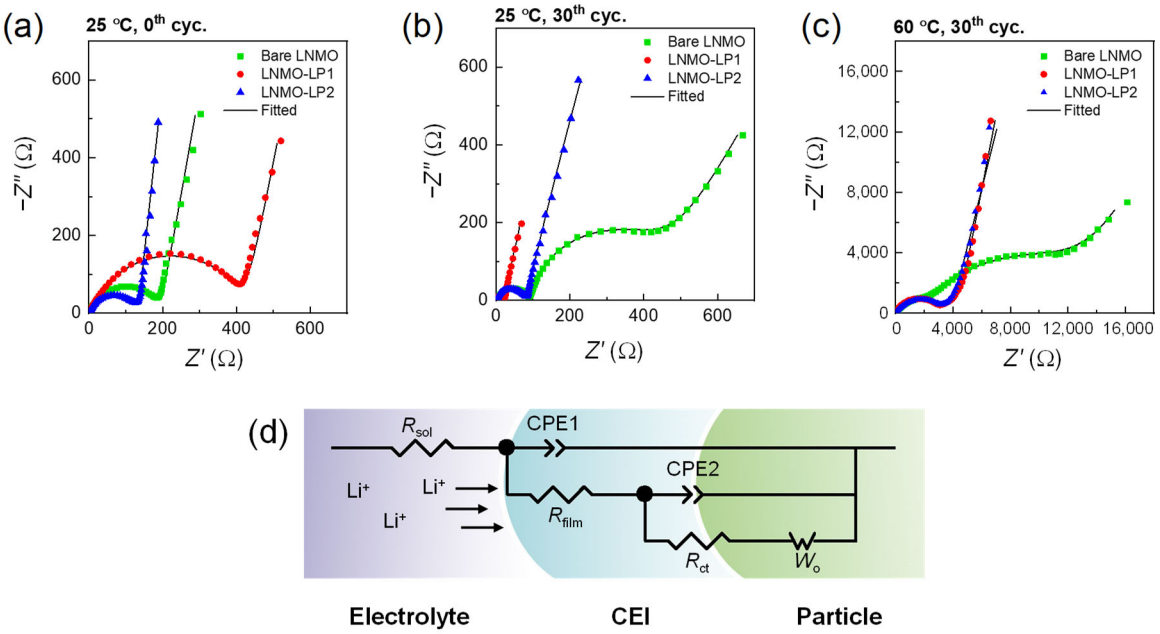



**Figure 8.** EIS spectra of LNMO cells (**a**) at the initial state, (**b**) after 30 cycles at 25 °C, and (**c**) after 30 cycles at 60 °C. (**d**) Equivalent circuit used for fitting the data. All EIS measurements were conducted at 25 °C using 1 M $LiPF_6$ in EC:EMC (3:7 *w*/*w*) as the electrolyte.

**Table 3.** Fitted parameters of EIS data after 30 cycles at 60 °C.

| | $R_{sol}$ (Ω) | $R_{film}$ (Ω) | $R_{ct}$ (Ω) |
|---|---|---|---|
| Bare LNMO | 3.31 | 2232 | 12,000 ± 8000 |
| LP1-LNMO | 6.6 ± 0.2 | 13 ± 6 | 2890 ± 20 |
| LP2-LNMO | 6.4 ± 0.2 | 550 ± 40 | 2440 ± 60 |

As a manganese-rich compound, LNMO is particularly vulnerable for the manganese dissolution because of Jahn–Teller distortion of $Mn^{3+}$ during the electrochemical operation. The high-voltage operation makes the manganese dissolution severe, and other side reactions at the higher voltage lead to the electrolyte starvation and the altered surface structure that is inactive for $Li^+$ (de)intercalation [72]. In addition, the high-temperature operation accelerates those side reactions including manganese dissolution and HF attack, resulting in extremely high charge transfer resistance for bare LNMO cathode [5,16,72]. $Li_3PO_4$ coating of LNMO cathodes effectively addresses those problems by protecting the surface from the side reactions such as HF attack, Mn dissolution, and electrolyte decomposition, resulting in improved electrochemical and thermal stability.

## 4. Conclusions

In this study, $Li_3PO_4$-coated $LiNi_{0.5}Mn_{1.5}O_4$ (LNMO) cathode materials were successfully synthesized via a simple wet-coating method. The formation of a stable $Li_3PO_4$ protective layer significantly enhanced the electrochemical performance of the cathodes. The surface coating not only improved cycling and rate capabilities but also effectively suppressed undesirable interfacial reactions between the LNMO cathode and the electrolyte, particularly under high-voltage and high-temperature conditions. The electrochemical impedance spectroscopy (EIS) results revealed that the 1 wt% $Li_3PO_4$ coating effectively reduced both film resistance and charge-transfer resistance, indicating excellent interfacial stability. These findings demonstrate that applying a $Li_3PO_4$ layer with controlled thickness can suppress side reactions and enhance charge-transfer kinetics of high-voltage spinel cathodes. This suggests a promising strategy for the development of next-generation lithium-ion batteries with higher energy density and improved safety. Furthermore, the simplicity and scalability of the proposed coating process indicate its potential applicability to industrial-scale electrode manufacturing. Future research should focus on further optimization of the coating thickness and uniformity, as well as exploring the compatibility of $Li_3PO_4$ coatings with other high-energy cathode materials and electrolytes. These efforts could provide deeper insight into interfacial stability and contribute to the advancement of durable and safe high-voltage lithium-ion batteries.

**Supplementary Materials:** The following supporting information can be downloaded at: https://www.mdpi.com/article/10.3390/en18133387/s1, Figure S1. SEM image of bare-LNMO electrode after the slurry coating on aluminum substrate. Figure S2. EDS patterns of (a) bare- and (b) LP1-LNMO. Figure S3. Elemental mapping of SEM images for (a) bare-LNMO and (b) LP1-LNMO. Table S1. Coulombic efficiency (%) of bare and Li3PO4-coated LiNi0.5Mn1.5O4 cathodes at different C-rates (0.05C and 1C) and temperatures (25 °C and 60 °C). Table S2. Warburg factor ($\sigma$) and corresponding diffusion coefficients ($D$), derived from the slope of the $Z_{real}$ vs $\omega^{-0.5}$ plots of the impedance data at 25 °C before cycling.

**Author Contributions:** Conceptualization, S.Y.C. and H.D.Y.; Methodology, S.Y.C., J.H.S. and F.H.; Investigation, S.Y.C., J.H.S., F.H., S.K.M. and M.K.S.; Writing—original draft, S.Y.C.; Writing—review & editing, S.K.M., M.K.S. and H.D.Y.; Supervision, H.D.Y.; Project administration, H.D.Y.; Funding acquisition, H.D.Y. All authors have read and agreed to the published version of the manuscript.

**Funding:** This work was supported by a two-year research grant of Pusan National University.

**Data Availability Statement:** The original contributions presented in this study are included in the article/Supplementary Materials. Further inquiries can be directed to the corresponding author.

**Conflicts of Interest:** The authors declare no conflict of interest.

## References


1. Li, L.; Sui, J.S.; Chen, J.; Lu, Y.C. $LiNi_{0.5}Mn_{1.5}O_4$ microrod with ultrahigh $Mn^{3+}$ content: A high performance cathode material for lithium ion battery. *Electrochim. Acta* **2019**, *305*, 433–442. [CrossRef]
2. Nisar, U.; Amin, R.; Essehli, R.; Shakoor, R.A.; Kahraman, R.; Kim, D.K.; Khaleel, M.A.; Belharouak, I. Extreme fast charging characteristics of zirconia modified $LiNi_{0.5}Mn_{1.5}O_4$ cathode for lithium ion batteries. *J. Power Sources* **2018**, *396*, 774–781. [CrossRef]
3. Xiao, J.; Chen, X.; Sushko, P.V.; Sushko, M.L.; Kovarik, L.; Feng, J.; Deng, Z.; Zheng, J.; Graff, G.L.; Nie, Z.; et al. High-Performance $LiNi_{0.5}Mn_{1.5}O_4$ Spinel Controlled by $Mn^{3+}$ Concentration and Site Disorder. *Adv. Mater.* **2012**, *24*, 2109–2116. [CrossRef] [PubMed]
4. Chong, J.; Zhang, J.; Xie, H.; Song, X.; Liu, G.; Battaglia, V.; Xun, S.; Wang, R. High performance $LiNi_{0.5}Mn_{1.5}O_4$ cathode material with a bi-functional coating for lithium ion batteries. *RSC Adv.* **2016**, *6*, 19245–19251. [CrossRef]
5. Yubuchi, S.; Ito, Y.; Matsuyama, T.; Hayashi, A.; Tatsumisago, M. 5V class $LiNi_{0.5}Mn_{1.5}O_4$ positive electrode coated with $Li_3PO_4$ thin film for all-solid-state batteries using sulfide solid electrolyte. *Solid State Ion.* **2016**, *285*, 79–82. [CrossRef]
6. Nasajpour-Esfahani, N.; Garmestani, H.; Bagheritabar, M.; Jasim, D.J.; Toghraie, D.; Dadkhah, S.; Firoozeh, H. Comprehensive review of lithium-ion battery materials and development challenges. *Renew. Sustain. Energy Rev.* **2024**, *203*, 114783. [CrossRef]
7. Yang, T.; Zhang, N.; Lang, Y.; Sun, K. Enhanced rate performance of carbon-coated $LiNi_{0.5}Mn_{1.5}O_4$ cathode material for lithium ion batteries. *Electrochim. Acta* **2011**, *56*, 4058–4064. [CrossRef]
8. Sha, O.; Wang, S.; Qiao, Z.; Yuan, W.; Tang, Z.; Xu, Q.; Su, Y. Synthesis of spinel $LiNi_{0.5}Mn_{1.5}O_4$ cathode material with excellent cycle stability using urea-based sol–gel method. *Mater. Lett.* **2012**, *89*, 251–253. [CrossRef]
9. Dong, H.; Zhang, Y.; Zhang, S.; Tang, P.; Xiao, X.; Ma, M.; Zhang, H.; Yin, Y.; Wang, D.; Yang, S. Improved High Temperature Performance of a Spinel $LiNi_{0.5}Mn_{1.5}O_4$ Cathode for High-Voltage Lithium-Ion Batteries by Surface Modification of a Flexible Conductive Nanolayer. *ACS Omega* **2019**, *4*, 185–194. [CrossRef]
10. Feng, S.; Kong, X.; Sun, H.; Wang, B.; Luo, T.; Liu, G. Effect of Zr doping on $LiNi_{0.5}Mn_{1.5}O_4$ with ordered or disordered structures. *J. Alloys Compd.* **2018**, *749*, 1009–1018. [CrossRef]
11. Wang, J.; Lin, W.; Wu, B.; Zhao, J. Syntheses and electrochemical properties of the Na-doped $LiNi_{0.5}Mn_{1.5}O_4$ cathode materials for lithium-ion batteries. *Electrochim. Acta* **2014**, *145*, 245–253. [CrossRef]
12. Santhanam, R.; Rambabu, B. Research progress in high voltage spinel $LiNi_{0.5}Mn_{1.5}O_4$ material. *J. Power Sources* **2010**, *195*, 5442–5451. [CrossRef]
13. Chang, Q.; Wei, A.; Li, W.; Bai, X.; Zhang, L.; He, R.; Liu, Z. Structural and electrochemical characteristics of $Al_2O_3$-modified $LiNi_{0.5}Mn_{1.5}O_4$ cathode materials for lithium-ion batteries. *Ceram. Int.* **2019**, *45*, 5100–5110. [CrossRef]
14. Chae, J.S.; Yoon, S.-B.; Yoon, W.-S.; Kang, Y.-M.; Park, S.-M.; Lee, J.-W.; Roh, K.C. Enhanced high-temperature cycling of $Li_2O$–$2B_2O_3$-coated spinel-structured $LiNi_{0.5}Mn_{1.5}O_4$ cathode material for application to lithium-ion batteries. *J. Alloys Compd.* **2014**, *601*, 217–222. [CrossRef]
15. Deng, Y.; Mou, J.; He, L.; Xie, F.; Zheng, Q.; Xu, C.; Lin, D. A core–shell structured $LiNi_{0.5}Mn_{1.5}O_4$@$LiCoO_2$ cathode material with superior rate capability and cycling performance. *Dalton Trans.* **2018**, *47*, 367–375. [CrossRef]
16. Shang, Y.; Lin, X.; Lu, X.; Huang, T.; Yu, A. Nano-$TiO_2$(B) coated $LiMn_2O_4$ as cathode materials for lithium-ion batteries at elevated temperatures. *Electrochim. Acta* **2015**, *156*, 121–126. [CrossRef]
17. Sun, Y.K.; Hong, K.J.; Prakash, J.; Amine, K. Electrochemical performance of nano-sized ZnO-coated $LiNi_{0.5}Mn_{1.5}O_4$ spinel as 5 V materials at elevated temperatures. *Electrochem. Commun.* **2002**, *4*, 344–348. [CrossRef]
18. Kim, H.; Byun, D.; Chang, W.; Jung, H.-G.; Choi, W. A nano-$LiNbO_3$ coating layer and diffusion-induced surface control towards high-performance 5 V spinel cathodes for rechargeable batteries. *J. Mater. Chem.* **2017**, *5*, 25077–25089. [CrossRef]
19. Sahan, H.; Goktepe, H.; Patat, S.; Ulgen, A. Effect of the $Cr_2O_3$ coating on electrochemical properties of spinel $LiMn_2O_4$ as a cathode material for lithium battery applications. *Solid State Ion.* **2010**, *181*, 1437–1444. [CrossRef]
20. Fan, Y.; Wang, J.; Tang, Z.; He, W.; Zhang, J. Effects of the nanostructured $SiO_2$ coating on the performance of $LiNi_{0.5}Mn_{1.5}O_4$ cathode materials for high-voltage Li-ion batteries. *Electrochim. Acta* **2007**, *52*, 3870–3875. [CrossRef]
21. Kim, J.W.; Kim, D.H.; Oh, D.Y.; Lee, H.; Kim, J.H.; Lee, J.H.; Jung, Y.S. Surface chemistry of $LiNi_{0.5}Mn_{1.5}O_4$ particles coated by $Al_2O_3$ using atomic layer deposition for lithium-ion batteries. *J. Power Sources* **2015**, *274*, 1254–1262. [CrossRef]
22. Hong, D.; Guo, Y.; Wang, H.; Zhou, J.; Fang, H.-T. Mechanism for improving the cycle performance of $LiNi_{0.5}Mn_{1.5}O_4$ by $RuO_2$ surface modification and increasing discharge cut-off potentials. *J. Mater. Chem.* **2015**, *3*, 15457–15465. [CrossRef]

23. Gao, X.-W.; Deng, Y.-F.; Wexler, D.; Chen, G.-H.; Chou, S.-L.; Liu, H.-K.; Shi, Z.-C.; Wang, J.-Z. Improving the electrochemical performance of the $LiNi_{0.5}Mn_{1.5}O_4$ spinel by polypyrrole coating as a cathode material for the lithium-ion battery. *J. Mater. Chem. A* **2015**, *3*, 404–411. [CrossRef]
24. Yi, T.-F.; Li, Y.-M.; Li, X.-Y.; Pan, J.-J.; Zhang, Q.; Zhu, Y.-R. Enhanced electrochemical property of $FePO_4$-coated $LiNi_{0.5}Mn_{1.5}O_4$ as cathode materials for Li-ion battery. *Sci. Bull.* **2017**, *62*, 1004–1010. [CrossRef]
25. Shchegolkov, A.V.; Lipkin, M.S.; Shchegolkov, A.V. Preparation of $WO_3$ Films on Titanium and Graphite Foil for Fuel Cell and Supercapacitor Applications by Electrochemical (Cathodic) Deposition Method. *Russ. J. Gen. Chem.* **2022**, *92*, 1161–1167. [CrossRef]
26. Liu, M.-H.; Huang, H.-T.; Lin, C.-M.; Chen, J.-M.; Liao, S.-C. Mg gradient-doped $LiNi_{0.5}Mn_{1.5}O_4$ as the cathode material for Li-ion batteries. *Electrochim. Acta* **2014**, *120*, 133–139. [CrossRef]
27. Lin, M.; Wang, S.H.; Gong, Z.L.; Huang, X.K.; Yang, Y. A Strategy to Improve Cyclic Performance of $LiNi_{0.5}Mn_{1.5}O_4$ in a Wide Voltage Region by Ti-Doping. *J. Electrochem. Soc.* **2013**, *160*, A3036–A3040. [CrossRef]
28. Zhong, G.B.; Wang, Y.Y.; Zhang, Z.C.; Chen, C.H. Effects of Al substitution for Ni and Mn on the electrochemical properties of $LiNi_{0.5}Mn_{1.5}O_4$. *Electrochim. Acta* **2011**, *56*, 6554–6561. [CrossRef]
29. Wang, H.; Tan, T.A.; Yang, P.; Lai, M.O.; Lu, L. High-Rate Performances of the Ru-Doped Spinel $LiNi_{0.5}Mn_{1.5}O_4$: Effects of Doping and Particle Size. *J. Phys. Chem. C* **2011**, *115*, 6102–6110. [CrossRef]
30. Mao, J.; Dai, K.; Xuan, M.; Shao, G.; Qiao, R.; Yang, W.; Battaglia, V.S.; Liu, G. Effect of Chromium and Niobium Doping on the Morphology and Electrochemical Performance of High-Voltage Spinel $LiNi_{0.5}Mn_{1.5}O_4$ Cathode Material. *ACS Appl. Mater. Interfaces* **2016**, *8*, 9116–9124. [CrossRef]
31. Kim, D.-J.; Ko, H.S.; Lee, J.-W. Lithium silicate–lithium phosphate ($xLi_4SiO_4-(1-x)Li_3PO_4$) coating on lithium nickel manganese oxide ($LiNi_{0.7}Mn_{0.3}O_2$) with a layered structure. *Solid State Ion.* **2015**, *278*, 239–244. [CrossRef]
32. Sung, J.H.; Kim, T.W.; Kang, H.K.; Choi, S.Y.; Hasan, F.; Mohanty, S.K.; Kim, J.; Srinivasa, M.K.; Shin, H.C.; Yoo, H.D. Superior high voltage $LiNi_{0.6}Co_{0.2}Mn_{0.2}O_2$ cathode using $Li_3PO_4$ coating for lithium-ion batteries. *Korean J. Chem. Eng.* **2021**, *38*, 1059–1065. [CrossRef]
33. Abebe, E.B.; Yang, C.-C.; Wu, S.-H.; Chien, W.-C.; Li, Y.-J.J. Surface modification with $Li_3PO_4$ enhances the electrochemical performance of $LiNi_{0.9}Co_{0.05}Mn_{0.05}O_2$ cathode materials for Li-Ion batteries. *J. Alloys Compd.* **2023**, *947*, 169455. [CrossRef]
34. Chen, T.; Yan, W.; Yu, D.; Ma, S.; Ma, L.; Huang, Q.; Li, N. Surface Modification of Micro-Silicon Anode for High-performance Lithium-Ion Batteries. *J. Phys. Conf. Ser.* **2023**, *2563*, 012017. [CrossRef]
35. Jiao, C.; Wang, M.; Huang, B.; Zhang, M.; Xu, G.; Liu, Y.; Zhao, Y.; Hu, X. Surface modification single crystal Li-rich $Li_{1.2}Mn_{0.54}Ni_{0.13}Co_{0.13}O_2$ as high performance cathode materials for Li-ion batteries. *J. Alloys Compd.* **2023**, *937*, 168389. [CrossRef]
36. Lee, J.Y.; Noh, S.; Seong, J.Y.; Lee, S.; Park, Y.J. Suppressing Unfavorable Interfacial Reactions Using Polyanionic Oxides as Efficient Buffer Layers: Low-Cost $Li_3PO_4$ Coatings for Sulfide-Electrolyte-Based All-Solid-State Batteries. *ACS Appl. Mater. Interfaces* **2023**, *15*, 12998–13011. [CrossRef]
37. Li, Y.; Zan, M.; Chen, P.; Huang, Y.; Xu, X.; Zhang, C.; Cai, Z.; Yu, X.; Li, H. Facile Solid-State Synthesis to In Situ Generate a Composite Coating Layer Composed of Spinel-Structural Compounds and $Li_3PO_4$ for Stable Cycling of $LiCoO_2$ at 4.6 V. *ACS Appl. Mater. Interfaces* **2023**, *15*, 51262–51273. [CrossRef]
38. Liang, J.; Zhu, Y.; Li, X.; Luo, J.; Deng, S.; Zhao, Y.; Sun, Y.; Wu, D.; Hu, Y.; Li, W.; et al. A gradient oxy-thiophosphate-coated Ni-rich layered oxide cathode for stable all-solid-state Li-ion batteries. *Nat. Commun.* **2023**, *14*, 146. [CrossRef]
39. Liu, X.; Weng, Q.; Liu, T.; Tang, Z.; Tang, H. A $Li_3PO_4$ coating strategy to enhance the Li-ion transport properties of $Li_2ZnTi_3O_8$ anode material for Lithium-ion Battery. *Electrochim. Acta* **2023**, *447*, 142151. [CrossRef]
40. Sun, Y.; Huang, W.; Zhao, G.; Liu, Q.; Duan, L.; Wang, S.; An, Q.; Wang, H.; Yang, Y.; Zhang, C.; et al. $LiNi_{0.9}Co_{0.09}Mo_{0.01}O_2$ Cathode with $Li_3PO_4$ Coating and Ti Doping for Next-Generation Lithium-Ion Batteries. *ACS Energy Lett.* **2023**, *8*, 1629–1638. [CrossRef]
41. Sun, Y.; Zhang, X.; Cheng, J.; Guo, M.; Li, X.; Wang, C.; Sun, L.; Yan, J. Surface modification with lithium-ion conductor $Li_3PO_4$ to enhance the electrochemical performance of lithium-rich layered $Li_{1.2}Ni_{0.2}Mn_{0.6}O_2$. *Ionics* **2023**, *29*, 2141–2152. [CrossRef]
42. Wang, Y.; Yu, W.; Zhao, L.; Wu, A.; Li, A.; Dong, X.; Huang, H. $AlPO_4$-$Li_3PO_4$ dual shell for enhancing interfacial stability of Co-free Li-rich Mn-based cathode. *Electrochim. Acta* **2023**, *462*, 142664. [CrossRef]
43. Zhao, S.; Ma, M.; Gao, L.; Gu, L.; Chen, M.; Han, G.; Yang, T.; Chen, J.; Qi, D.; Wang, P.; et al. Engineering the Li-ion flux and interfacial chemistry toward a stable Li metal anode via a simple separator coating strategy. *New J. Chem.* **2023**, *47*, 7986–7994. [CrossRef]
44. Sung, J.H.; Kim, T.; Kim, S.; Hasan, F.; Mohanty, S.K.; Srinivasa, M.K.; Reddy, S.C.; Yoo, H.D. $Li_3PO_4$-Coated Graphite Anode for Thermo-Electrochemically Stable Lithium-Ion Batteries. *Energies* **2023**, *16*, 6141. [CrossRef]
45. Dutta, J.; Ghosh, S.; Martha, S.K. Transforming Residual Lithium Compounds on the $LiNi_{0.8}Mn_{0.1}Co_{0.1}O_2$ Surface into a Li-Mn-P-O-Based Composite Coating for Multifaceted Improvements. *ACS Appl. Mater. Interfaces* **2024**, *16*, 19720–19729. [CrossRef]

46. Huang, K.; Xie, T.; Yang, H.; Zhou, J.; Lan, T.; Ong, S.; Jiang, H.; Zeng, Y.; Guo, H.; Zhang, Y. Plasma-assisted sputter $Li_3PO_4$ coating on NCM955 cathodes enhancing high-temperature cycling performances. *J. Alloys Compd.* **2024**, *976*, 173232. [CrossRef]
47. Kim, J.; Ku, M.; Kim, S.; Yang, H.; Lee, D.; Lee, H.; Kim, Y.-B. Interdiffusion suppression at the cathode-electrolyte interface of all-solid-state-batteries by $Li_3PO_4$ conformal coating. *J. Am. Ceram. Soc.* **2024**, *107*, 3134–3145. [CrossRef]
48. Li, Z.; Yi, H.; Li, X.; Gao, P.; Zhu, Y. Enhancing the Cycling and Rate Performance of Ni-Rich Cathodes for Lithium-Ion Batteries by Bulk-Phase Engineering and Surface Reconstruction. *ACS Appl. Mater. Interfaces* **2024**, *16*, 28537–28549. [CrossRef]
49. Shen, L.; Gu, Y.; Xu, T.; Zhou, Q.; Peng, P.; Chen, Y.; Du, F.; Zheng, J. Dual modification of phosphate toward improving electrochemical performance of $LiNiO_2$ cathode materials. *J. Colloid Interface Sci.* **2024**, *662*, 505–515. [CrossRef]
50. Wang, C.; Xie, Y.; Huang, Y.; Zhou, S.; Xie, H.; Jin, H.; Ji, H. $Li_3PO_4$-Enriched SEI on Graphite Anode Boosts Li+ De-Solvation Enabling Fast-Charging and Low-Temperature Lithium-Ion Batteries. *Angew. Chem. Int. Ed.* **2024**, *63*, e202402301. [CrossRef]
51. Xu, M.; Sheng, B.; Cheng, Y.; Lu, J.; Chen, M.; Wang, P.; Liu, B.; Chen, J.; Han, X.; Wang, M.-S.; et al. One-step calcination synthesis of interface-coherent crystallized and surface-passivated $LiNi_{0.5}Mn_{1.5}O_4$ for high-voltage lithium-ion battery. *Nano Res.* **2024**, *17*, 4192–4202. [CrossRef]
52. Xiao, W.; Wang, J.-L.; Yi, Z.-C.; Liu, C.-J.; Miao, C.; Xin, Y.; Nie, S.-Q. Dual modification of $LiNi_{0.83}Co_{0.11}Mn_{0.06}O_2$ cathode materials by $K^+$ doping and $Li_3PO_4$ coating for lithium ions batteries. *Rare Met.* **2024**, *43*, 3007–3018. [CrossRef]
53. Zhu, X.; Lin, Z.; Lai, J.; Lv, T.; Lin, T.; Pan, H.; Feng, J.; Wang, Q.; Han, S.; Chen, R.; et al. Highly Efficient Spatially-Temporally Synchronized Construction of Robust $Li_3PO_4$-rich Solid-Electrolyte Interphases in Aqueous Li-ion Batteries. *Angew. Chem. Int. Ed.* **2024**, *63*, e202317549. [CrossRef] [PubMed]
54. Jiang, Q.; Li, X.; Hao, Y.; Zuo, J.; Duan, R.; Li, J.; Cao, G.; Wang, J.; Wang, J.; Li, M.; et al. Oxygen-Vacancy-Assisted Dual Functional Surface Coatings Suppressing Irreversible Phase Transition of Li-Rich Layered Oxide Cathodes. *Adv. Funct. Mater.* **2025**, *35*, 2400670. [CrossRef]
55. Miyashiro, H.; Seki, S.; Kobayashi, Y.; Ohno, Y.; Mita, Y.; Usami, A. All-solid-state lithium polymer secondary battery with $LiNi_{0.5}Mn_{1.5}O_4$ by mixing of $Li_3PO_4$. *Electrochem. Commun.* **2005**, *7*, 1083–1086. [CrossRef]
56. Chong, J.; Xun, S.; Zhang, J.; Song, X.; Xie, H.; Battaglia, V.; Wang, R. $Li_3PO_4$-Coated $LiNi_{0.5}Mn_{1.5}O_4$: A Stable High-Voltage Cathode Material for Lithium-Ion Batteries. *Chem. Eur. J.* **2014**, *20*, 7479–7485. [CrossRef]
57. Konishi, H.; Suzuki, K.; Taminato, S.; Kim, K.; Zheng, Y.; Kim, S.; Lim, J.; Hirayama, M.; Son, J.-Y.; Cui, Y.; et al. Effect of surface $Li_3PO_4$ coating on $LiNi_{0.5}Mn_{1.5}O_4$ epitaxial thin film electrodes synthesized by pulsed laser deposition. *J. Power Sources* **2014**, *269*, 293–298. [CrossRef]
58. Hallot, M.; Caja-Munoz, B.; Leviel, C.; Lebedev, O.I.; Retoux, R.; Avila, J.; Roussel, P.; Asensio, M.C.; Lethien, C. Atomic Layer Deposition of a Nanometer-Thick $Li_3PO_4$ Protective Layer on $LiNi_{0.5}Mn_{1.5}O_4$ Films: Dream or Reality for Long-Term Cycling? *ACS Appl. Mater. Interfaces* **2021**, *13*, 15761–15773. [CrossRef]
59. Mereacre, V.; Bohn, N.; Stueble, P.; Pfaffmann, L.; Binder, J.R. Instantaneous Surface $Li_3PO_4$ Coating and Al-Ti Doping and Their Effect on the Performance of $LiNi_{0.5}Mn_{1.5}O_4$ Cathode Materials. *ACS Appl. Energy Mater.* **2021**, *4*, 4271–4276. [CrossRef]
60. Wu, Y.; Ben, L.; Zhan, Y.; Yu, H.; Qi, W.; Zhao, W.; Huang, X. Binding $Li_3PO_4$ to Spinel $LiNi_{0.5}Mn_{1.5}O_4$ via a Surface Co-Containing Bridging Layer to Improve the Electrochemical Performance. *Energy Technol.* **2021**, *9*, 2100147. [CrossRef]
61. Shapira, A.; Tiurin, O.; Solomatin, N.; Auinat, M.; Meitav, A.; Ein-Eli, Y. Robust $AlF_3$ Atomic Layer Deposition Protective Coating on $LiMn_{1.5}Ni_{0.5}O_4$ Particles: An Advanced Li-Ion Battery Cathode Material Powder. *ACS Appl. Energy Mater.* **2018**, *1*, 6809–6823. [CrossRef]
62. Hallot, M.; Roussel, P.; Lethien, C. Sputtered $LiNi_{0.5}Mn_{1.5}O_4$ Thin Films for Lithium-Ion Microbatteries. *ACS Appl. Energy Mater.* **2021**, *4*, 3101–3109. [CrossRef]
63. Xia, H.; Meng, Y.S.; Lu, L.; Ceder, G. Electrochemical Properties of Nonstoichiometric $LiNi_{0.5}Mn_{1.5}O_{4-\delta}$ Thin-Film Electrodes Prepared by Pulsed Laser Deposition. *J. Electrochem. Soc.* **2007**, *154*, A737. [CrossRef]
64. Xia, H.; Tang, S.B.; Lu, L.; Meng, Y.S.; Ceder, G. The influence of preparation conditions on electrochemical properties of $LiNi_{0.5}Mn_{1.5}O_4$ thin film electrodes by PLD. *Electrochim. Acta* **2007**, *52*, 2822–2828. [CrossRef]
65. Duncan, H.; Abu-Lebdeh, Y.; Davidson, I. Study of the Cathode-Electrolyte Interface of $LiMn_{1.5}Ni_{0.5}O_4$ Synthesized by a Sol-Gel Method for Li-Ion Batteries. *J. Electrochem. Soc.* **2010**, *157*, A528. [CrossRef]
66. Kunduracı, M.; Amatucci, G. The effect of particle size and morphology on the rate capability of 4.7 V $LiMn_{1.5+\delta}Ni_{0.5-\delta}O_4$ spinel lithium-ion battery cathodes. *Electrochim. Acta* **2008**, *53*, 4193–4199. [CrossRef]
67. Song, M.Y.; Lee, R. Synthesis by sol–gel method and electrochemical properties of $LiNiO_2$ cathode material for lithium secondary battery. *J. Power Sources* **2002**, *111*, 97–103. [CrossRef]
68. Mokhtar, N.; Idris, N.H. Comparison on Electrochemical Performances of $LiNi_{0.5}Mn_{1.5}O_4$ Cathode Materials Synthesized Using Different Precursors. *Mater. Today* **2016**, *3*, S129–S135. [CrossRef]
69. Hao, Y.-J.; Lai, Q.-Y.; Liu, D.-Q.; Xu, Z.-U.; Ji, X.-Y. Synthesis by citric acid sol–gel method and electrochemical properties of $Li_4Ti_5O_{12}$ anode material for lithium-ion battery. *Mater. Chem. Phys.* **2005**, *94*, 382–387. [CrossRef]

70. Lee, Y.S.; Sun, Y.K.; Ota, S.; Miyashita, T.; Yoshio, M. Preparation and characterization of nano-crystalline $LiNi_{0.5}Mn_{1.5}O_4$ for 5 V cathode material by composite carbonate process. *Electrochem. Commun.* **2002**, *4*, 989–994. [CrossRef]
71. Song, H.G.; Kim, J.Y.; Kim, K.T.; Park, Y.J. Enhanced electrochemical properties of $Li(Ni_{0.4}Co_{0.3}Mn_{0.3})O_2$ cathode by surface modification using $Li_3PO_4$-based materials. *J. Power Sources* **2011**, *196*, 6847–6855. [CrossRef]
72. Chen, S.; He, T.; Su, Y.; Lu, Y.; Bao, L.; Chen, L.; Zhang, Q.; Wang, J.; Chen, R.; Wu, F. Ni-Rich $LiNi_{0.8}Co_{0.1}Mn_{0.1}O_2$ Oxide Coated by Dual-Conductive Layers as High Performance Cathode Material for Lithium-Ion Batteries. *ACS App. Mater. Interfaces* **2017**, *9*, 29732–29743. [CrossRef]
73. Bläubaum, L.; Röder, F.; Nowak, C.; Chan, H.S.; Kwade, A.; Krewer, U. Impact of Particle Size Distribution on Performance of Lithium-Ion Batteries. *ChemElectroChem* **2020**, *7*, 4755–4766. [CrossRef]
74. Zhang, J.; Qiao, J.; Sun, K.; Wang, Z. Balancing particle properties for practical lithium-ion batteries. *Particuology* **2022**, *61*, 18–29. [CrossRef]
75. Jang, J.; Chen, Y.-T.; Deysher, G.; Cheng, D.; Ham, S.-Y.; Cronk, A.; Ridley, P.; Yang, H.; Sayahpour, B.; Han, B.; et al. Enabling a Co-Free, High-Voltage LiNi0.5Mn1.5O4 Cathode in All-Solid-State Batteries with a Halide Electrolyte. *ACS Energy Lett.* **2022**, *7*, 2531–2539. [CrossRef]
76. Mou, M.; Patel, A.; Mallick, S.; Thapaliya, B.P.; Paranthaman, M.P.; Mugumya, J.H.; Rasche, M.L.; Gupta, R.B.; Saleh, S.; Kothe, S.; et al. Scalable Advanced Li(Ni0.8Co0.1Mn0.1)O2 Cathode Materials from a Slug Flow Continuous Process. *ACS Omega* **2022**, *7*, 42408–42417. [CrossRef]
77. Wang, S.; Zhu, J.; Li, Y.; Cao, G.; Chen, Y.; Zhang, D.; Tan, Z.; Yang, J.; Zheng, J.; Li, H. Role of Al on the electrochemical performances of quaternary nickel-rich cathode $LiNi_{0.8}Co_{0.1}Mn_{0.1-x}Al_xO_2$ ($0 \leq x \leq 0.06$) for lithium-ion batteries. *J. Electroanal. Chem.* **2021**, *888*, 115200. [CrossRef]
78. Jo, C.-H.; Cho, D.-H.; Noh, H.-J.; Yashiro, H.; Sun, Y.-K.; Myung, S.T. An effective method to reduce residual lithium compounds on Ni-rich $Li[Ni_{0.6}Co_{0.2}Mn_{0.2}]O_2$ active material using a phosphoric acid derived $Li_3PO_4$ nanolayer. *Nano Res.* **2015**, *8*, 1464–1479. [CrossRef]
79. Wu, H.M.; Belharouak, I.; Abouimrane, A.; Sun, Y.K.; Amine, K. Surface modification of $LiNi_{0.5}Mn_{1.5}O_4$ by $ZrP_2O_7$ and $ZrO_2$ for lithium-ion batteries. *J. Power Sources* **2010**, *195*, 2909–2913. [CrossRef]


**Disclaimer/Publisher's Note:** The statements, opinions and data contained in all publications are solely those of the individual author(s) and contributor(s) and not of MDPI and/or the editor(s). MDPI and/or the editor(s) disclaim responsibility for any injury to people or property resulting from any ideas, methods, instructions or products referred to in the content.